NASA TN D-878

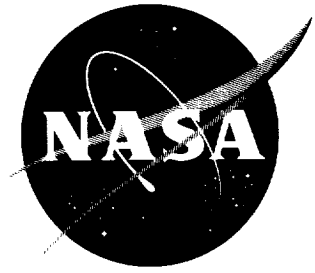

TECHNICAL NOTE

D-878

ANALYSIS, FEASIBILITY, AND WALL-TEMPERATURE DISTRIBUTION OF A RADIATION-COOLED NUCLEAR-ROCKET NOZZLE

By William H. Robbins and Carroll A. Todd

Lewis Research Center
Cleveland, Ohio

NATIONAL AERONAUTICS AND SPACE ADMINISTRATION
WASHINGTON

January 1962

NATIONAL AERONAUTICS AND SPACE ADMINISTRATION

TECHNICAL NOTE D-878

ANALYSIS, FEASIBILITY, AND WALL-TEMPERATURE DISTRIBUTION OF A RADIATION-COOLED NUCLEAR-ROCKET NOZZLE

By William H. Robbins and Carroll A. Todd

SUMMARY

An analysis was made to determine the feasibility of operating radiation-cooled nuclear-rocket nozzles with hydrogen as the propellant. Wall-temperature distributions and heat fluxes along the nozzle were calculated by two techniques. One wall-temperature distribution was obtained from a simplified heat balance which included only the convection into the wall and the radiation from the wall. A more refined calculation was made for wall temperature in which the heat balance included, in addition to the convection to and radiation from the wall, the radiation inside the nozzle and the axial and radial heat conduction. The agreement between the two solutions of temperature distribution was excellent in the divergent portion of the nozzle. The average temperature difference over the range of pressure and area ratio investigated was approximately 1 percent. In the convergent section large differences in temperature between the two solutions were observed, because the radiant heat flux from the reactor to the nozzle was neglected in the simplified solution.

At chamber pressures associated with nuclear-rocket design (400 lb/sq in.) the wall temperature (4400° R) at the throat approached the rocket chamber temperature. At an area ratio of 60 the wall temperature was approximately 2300° R. The wall temperatures increased at higher values of chamber pressure and, of course, decreased at lower values of chamber pressure. Increasing the outside wall emissivity decreased the wall temperature. In contrast, variations in the inside nozzle wall emissivity had little effect on the wall temperature. In view of the wall-temperature level, nozzle liners with low thermal conductivity that are capable of withstanding high gas temperatures are necessary to provide a thermal barrier for the nozzle wall structural material. Maximum liner thicknesses (at the throat) varied from 1 inch for steel pressure shells to 0.1 inch for refractory-metal pressure shells.

Obviously, in the range of wall temperatures associated with radiation-cooled nuclear nozzles (2000° to 4400° R), both nozzle material selection and fabrication will be difficult. However, since radiation-cooled nozzles are simpler in concept and will probably result in performance gains in terms of specific impulse over regeneratively cooled nozzles, and because of the anticipated difficulty of regenerative cooling at high chamber pressure, a development effort appears to be desirable.

INTRODUCTION

Radiation-cooled rocket nozzles are characterized by the fact that heat transferred from the propellant to the nozzle wall is directly radiated to space rather than transferred to a coolant flowing around the nozzle wall. Uncooled or radiation-cooled nuclear-rocket nozzles would be desirable from several standpoints. Uncooled rockets are simpler in concept in that no special provisions for cooling the nozzle are necessary. This fact may be particularly appealing in view of the results of reference 1, which indicate that it will be difficult to regeneratively cool nuclear-rocket nozzles with hydrogen as a propellant. Uncooled nozzles will also have a performance advantage over regeneratively cooled nozzles. Since the nozzle pressure loss will be eliminated, the turbopump pressure and propellant bleed requirements will be reduced, which will result in an increase in specific impulse. The magnitude of the impulse gain will depend on the particular vehicle and mission requirements.

Radiation-cooled nozzles have been considered in the past and appear to be a promising technique for chemical rockets with low chamber pressures and low heat-flux rates (ref. 2). This report (like ref. 2) presents the results of an analysis of a radiation-cooled nozzle. The application was, however, directed toward the nuclear rocket, and the calculation procedure was considerably more detailed than that of reference 2. The purpose of the investigation was twofold. Initially, it was felt that a comparison between simplified techniques and more refined methods of calculating nozzle wall temperature and heat-flux distributions would be desirable, and such a comparison is presented herein. In addition, it was desired to determine the feasibility of operating a radiation-cooled nuclear-rocket nozzle with hydrogen as the propellant. Therefore, wall-temperature distributions and heat fluxes were determined and presented for a fixed nozzle geometry over a range of chamber pressure and wall emissivity.

SYMBOLS

A area, sq in.

B combined radiant heat flux (emission plus reflection) leaving a particular element, Btu/(sec)(sq in.)

b wall thickness, in.

c_p	specific heat at constant pressure, Btu/(lb)(^oR)
d	diameter, in.
F	view factor
H	combined heat flux (emission plus reflection) arriving at a particular element, Btu/(sec)(sq in.)
h	heat-transfer coefficient, Btu/(sec)(sq in.)(^oR)
I	specific-impulse gain
k	thermal conductivity, Btu/(sec)(in.)(^oR)
l	length, in.
Δl	nozzle element length, in.
P	pressure
Pr	Prandtl number, $c_p\mu/k$
Q	heat flow, Btu/sec
q	heat flux, Btu/(sec)(sq in.)
R	distance between two area elements
Re	Reynolds number, $\rho Vd/\mu$
r	radius, in.
T	temperature, ^oR
V	velocity, in./sec
W	propellant flow, lb/sec
β	angle between normal to surface area element and line connecting two surface area elements
ϵ	emissivity

η angle between surface area element and axis

θ angular coordinate (fig. 2)

μ viscosity, lb/(sec)(in.)

ρ density, lb/cu in.

σ Stephan-Boltzmann constant, 3.34×10^{-15} Btu/(sec)(sq in.)($^{\circ}R^4$)

Subscripts:

a axial conduction

ad adiabatic wall

an wall cross section

b stream conditions

C convection

c chamber or stagnation conditions

h hydraulic

i inside

in into element

n element under consideration

o outside

out out of element

r radiation

ref reference temperature

S surface

t total

w wall

γ gamma heating

θ external source

Superscript:

* nozzle throat conditions

ANALYSIS

The analysis was directed toward the nuclear rocket, and it was assumed that the nozzle propellant was hydrogen. A schematic diagram of the nuclear-rocket nozzle is shown in figure 1. The propellant flows through the reactor, where it is heated to temperatures of 4000° to 5000° R. The hydrogen then passes into the nozzle and is expanded to supersonic velocities and thus produces propulsive thrust. The analysis approach and the analytical procedures used to determine nozzle wall-temperature distributions and heat fluxes are presented in this section of the report.

Heat Balance

If a small-volume element of the nozzle wall is considered, the total heat input to the wall element is the sum of heat inputs from the following several sources: (1) the heat convection from the propellant to the wall, (2) the thermal radiation from the reactor to the wall and from one wall element to another, (3) the axial heat conduction in the wall from element to element, (4) the thermal radiation from outside sources such as the sun or other celestial bodies, and (5) the nuclear (gamma) heating from the reactor. The total heat input in equation form can be expressed as

$$Q_{t,in} = Q_{c,in} + Q_{r,in} + Q_{a,in} + Q_{\theta,in} + Q_{\gamma,in} \tag{1}$$

The total heat output of a typical volume element arises from two sources, (1) the heat radiated from the volume element, and (2) the heat conduction from one element to another:

$$Q_{t,out} = Q_{r,out} + Q_{a,out} \tag{2}$$

Defining the net heat input Q_t as the difference between the total heat output and the total heat input and subtracting equation (1) from

equation (2) result in

$$Q_t = Q_{t,out} - Q_{t,in} = - Q_{C,in} + Q_r + Q_a - Q_{\theta,in} - Q_{\gamma,in} \qquad (3)$$

Since the steady-state solution (the situation where the wall temperature does not vary with time) is desired, the net heat input is zero, and the equation to be solved for temperature is

$$-Q_{C,in} + Q_r + Q_a - Q_{\theta,in} - Q_{\gamma,in} = 0 \qquad (4)$$

As in the case of a regeneratively cooled rocket (ref. 1), it was felt that the gamma heating $Q_{\gamma,in}$ would be a small percentage of the total heat flux, and therefore $Q_{\gamma,in}$ was neglected in this analysis. However, it should be noted that, since total heat flux associated with the radiation-cooled nozzles will be significantly less than the values associated with regeneratively cooled nozzles, the nuclear heating will represent a larger percentage of the total heat load and therefore may become significant for nozzles with thick walls operating at high chamber pressures. In addition, the radiant energy from external sources $Q_{\theta,in}$ was also neglected. If the nozzle wall temperature is relatively high (above 1500° R), external radiation from the sun and other sources is negligible. Nozzle wall temperatures are usually above this level. Therefore, with both gamma heating and external radiation omitted, equation (4) becomes

$$-Q_{C,in} + Q_r + Q_a = 0 \qquad (5)$$

Equation (5) was expressed in terms of and solved for wall temperature. The technique of handling each term and the method of solution is described in the remaining part of the analysis section.

Convective Heat Transfer

The convective heat-transfer coefficient from the propellant to the nozzle wall with fully developed turbulent pipe flow assumed (ref. 3, ch. 8) is

$$h = 0.0265 \frac{k}{d_h} (Re)^{0.8}(Pr)^{0.33} \qquad (6)$$

Equation (6) can be rewritten in the following form:

$$h = \frac{0.0265(\rho V_b)^{0.8} c_p \mu^{0.2}}{d_h^{0.2}(Pr)^{0.67}} \qquad (7)$$

Utilizing the perfect gas law, the continuity equation, and, as recommended in reference 3 (p. 177), evaluating the transport properties (c_p, μ, and k) and the density ρ at a reference temperature, equation (7) becomes

$$h = \frac{0.026\left(\frac{W}{A}\right)^{0.8} c_{p,ref}\mu_{ref}^{0.2}}{d_h^{0.2}(Pr)_{ref}^{0.67}}\left(\frac{T_b}{T_{ref}}\right)^{0.8} \tag{8}$$

where the reference temperature is defined as

$$T_{ref} = 0.5\ T_{w,i} + 0.5\ T_b + 0.22(Pr)^{1/3}(T_c - T_b) \tag{9}$$

For the range of reference temperature encountered in this analysis (800° to 3000° R), reference 4 indicates that both specific heat c_p and Prandtl number Pr are relatively insensitive to variations in temperature and pressure. Therefore, average values of specific heat and Prandtl number were selected and held constant throughout the analysis. The values were $Pr = 0.80$ and $c_p = 3.70$ Btu/(lb)(°R). In addition it was found from reference 4 that variations in viscosity were closely approximated by the relation

$$\mu_{ref} = T_{ref}^{0.63}\times 10^{-8} \tag{10}$$

Substituting for Prandtl number, specific heat, and viscosity and expressing the diameter in terms of area yield for equation (8)

$$h = \frac{0.0028\ W^{0.8}T_b^{0.8}}{\left(\frac{A}{A^*}\right)^{0.9}(A^*)^{0.9}(T_{ref})^{0.67}} \tag{11}$$

Equation (11) was used for all computations of heat-transfer coefficient throughout the analysis. The variation of stream temperature T_b with area ratio was obtained from aerodynamic considerations only (ref. 4). As is customary in rocket nozzle heat-transfer calculations, it was assumed that the propellant stream temperature was not affected by the heat transfer to the wall. The convective heat flux q_c was then determined from

$$q_c = h(T_{ad} - T_{w,i}) \tag{12}$$

where

$$T_{ad} = T_b + (Pr)_{ref}^{1/3}(T_c - T_b) \tag{13}$$

The expression for adiabatic wall temperature (eq. (13)) was approximated by

$$T_{ad} = 0.9\ T_c + 0.1\ T_b \tag{13a}$$

for all calculations. The total convective heat flow for a particular volume element Q_C is

$$Q_C = q_C A_{S,i} \tag{14}$$

Radiant Heat Transfer

The radiant heat transfer from one nozzle element to another was determined on both inner and outer walls. The computation consists of two phases. First the view factor from one nozzle surface area element to another must be evaluated. The view factor is defined as that fraction of the total radiation leaving one surface area element which arrives at any other surface area element. The final phase of the calculation consists of the determination of the radiant heat flux from the view factors, specified surface temperatures, and emissivities. This computation is described in detail for the inside wall in reference 5 and is briefly reviewed here.

Since the rocket nozzle is a surface of revolution, the view factor of a perfectly general surface of revolution was derived so that it could be applied to any nozzle shape. The view factor from a point source to a finite area in terms of the cylindrical coordinate system shown in figure 2 can be expressed as

$$F_{dA_n \to A} = \frac{1}{\pi} \int_l \frac{dl}{\cos \eta} \int_\theta \frac{(\cos \beta_n)(\cos \beta)}{R^2}\, r\, d\theta \tag{15}$$

where R is the distance between the two differential areas dA_n and dA and the angles β and β_n are measured between the distance R and the respective normals to the differential areas. The angles β and β_n and the distance R were expressed in terms of the quantities r, θ, and l of the cylindrical coordinate system. The nozzle was divided into a number of finite segments (fig. 3), and the integral with respect to θ was integrated directly at each point along the nozzle. The integral with respect to l was evaluated numerically for each segment. Summation of the view factors for each finite segment was taken as the solution of equation (15).

As indicated in reference 5, because of the convergent-divergent geometry, the line of sight from one nozzle element to another is often completely or partly blocked, and the θ limits of integration vary over the length of the nozzle. The expression for determining the limits of integration on the inside of the nozzle is presented in reference 5. For the outside surface of the nozzle the same expression for the view factor (eq. (15)) applies; however, the limits of integration were determined to be the minimum angle obtained from either

$$\theta = \cos^{-1}\left(\frac{r + l \tan \eta}{r_n}\right) \tag{16}$$

or

$$\theta = \cos^{-1}\left(\frac{r_n - l \tan \eta_n}{r}\right) \tag{16a}$$

The radiation B_n leaving a particular surface element n per unit area per unit time is combined emission and reflection and can be expressed as

$$B_n = e_n + (1 - \epsilon_n)H_n \tag{17}$$

where H_n is the incoming energy from all the other surfaces that impinge on surface n, and e_n, the emitted energy from surface n, is defined by

$$e_n = \epsilon_n \sigma T_n^4 \tag{18}$$

The energy H_n is related to the energy leaving the other surfaces B_1, B_2, . . . B_n. If it is assumed that the temperature, emissivity, and reflectivity are constant over any surface n,

$$H_n = B_1F_{n-1} + B_2F_{n-2} + \ldots + B_nF_{n-n} \tag{19}$$

Combining equations (19) and (17) yields

$$(1 - \epsilon_n)F_{n-1}B_1 + (1 - \epsilon_n)F_{n-2}B_2 + \ldots + [(1 - \epsilon_n)F_{n-n} - 1]B_n = -e_n \tag{20}$$

Letting $n = 1, 2, 3 \ldots$ in equation (20) results in a system of algebraic equations that can be solved simultaneously for $B_1, B_2, \ldots B_n$ when the temperatures and emissivities of the n surfaces are assigned.

Since the net radiant heat transfer is the difference between the incoming and outgoing energy, it may be expressed as

$$q_{r,n} = B_n - H_n \tag{21}$$

or by combining equation (17) with (21)

$$q_{r,n} = \frac{e_n - \epsilon_n B_n}{1 - \epsilon_n} \tag{22}$$

and

$$Q_{r,n} = A_S q_{r,n} \tag{23}$$

Axial Conduction

In addition to the convection and radiation heat transfer, heat is conducted through the wall in both axial and radial directions. Proper evaluation of the conduction heat transfer, therefore, requires a two-dimensional solution of the heat conduction equation. In this analysis it was felt that the heat conduction would not appreciably affect the wall-temperature distributions or heat-transfer rates, and therefore the rather extensive effort required to obtain a two-dimensional conduction solution was not felt to be justified. The wall heat conduction was not ignored completely, however. It was assumed that the required two-dimensional solution could be approximated by one-dimensional solutions in both axial and radial directions.

For a typical nozzle element n the axial heat conduction Q_a into the element can be expressed as

$$Q_{a,in,n} = -k_w A_{an,n} \left(\frac{dT}{dl}\right)_n \tag{24}$$

where $A_{an,n}$ is the nozzle wall cross-sectional area and k_w is the thermal conductivity of the wall material. The axial conduction out of the element is

$$Q_{a,out,n} = Q_{a,in,n} + \frac{dQ_a}{dl}\, dl \tag{25}$$

Subtracting equation (24) from (25) gives the net axial conduction for a particular element

$$Q_a = -k_w A_{an,n} \left(\frac{d^2T}{dl^2}\right)_n dl \tag{26}$$

Equation (26) expressed in finite difference form is

$$Q_a = -k_w A_{an,n} \Delta l \left[\frac{T_{n+1} - 2T_n + T_{n-1}}{(\Delta l)^2}\right] \tag{27}$$

or

$$Q_a = -\frac{k_w A_{an,n}}{\Delta l}(T_{n+1} - 2T_n + T_{n-1}) \tag{28}$$

Equation (28) was utilized for evaluating the axial conduction term. Temperatures were taken as the inside wall temperature, and, as initial boundary conditions, the inlet and exit ends of the nozzle were assumed to be insulated (no heat transfer to the external environment was occurring).

One-dimensional radial conduction was also taken into account in the calculation of the outside wall temperature, and this discussion is included in the next section.

Procedure

In order to solve the heat balance equation for the wall-temperature distribution, the convection, radiation, and axial conduction terms in equations (14), (23), and (28) were substituted into the heat balance equation (eq. (5)), with the result (for a particular element n)

$$-h(T_{ad} - T_{w,i})A_{S,i} + \left(\frac{e - \epsilon B}{1 - \epsilon}\right)_o A_{s,o} + \left(\frac{e - \epsilon B}{1 - \epsilon}\right)_i A_{s,i} - A_{an}\frac{k_w}{\Delta l}(T_{n+1} - 2T_n + T_{n-1}) = 0 \tag{29}$$

The radiation terms are functions of the fourth power of the wall temperature, and the convection and conduction terms are linear functions of the wall temperature; therefore, equation (29) is a nonlinear fourth-degree equation and no direct solution can be obtained. Therefore, trial-and-error procedures were used to solve for the temperature distribution.

The straight-line nozzle shown in figure 3 was used in the analysis. Since the nozzle shape was very similar to the one utilized in reference 1, the same variations in propellant flow and chamber pressure apply and were used in the calculations of the temperature distributions. Inasmuch as small variations in wall-temperature distribution were expected with variations in nozzle geometry, the nozzle shape was held constant throughout the analysis. The emissivity of the reactor face was chosen equal to that of the inside wall, and the reactor face temperature was taken to be equal to the propellant chamber temperature (4680° R). The nozzle was divided into 41 segments as shown in figure 3, and an initial inside wall-temperature distribution $T_{w,i}$ was assumed. (The method of choosing the initial temperature distribution is discussed in detail later.) The net heat flow into the inside wall Q_i (radiation plus the convection) was then calculated from equations (14) and (23). With the specification of the wall thickness and thermal conductivity, the outside wall temperature was determined from

$$T_{w,o} = \frac{-bQ_i}{A_{S,i}k_w} + T_{w,i} \tag{30}$$

The outside wall radiation heat flux was determined from the outside wall temperature, and the individual heat flow terms were substituted into equation (29). If equation (29) was greater than zero, the inside wall temperature was decreased; conversely if equation (29) became negative, the temperature was increased. Fortunately, no real difficulty was encountered in making the solution converge, because the initial specification of inside wall temperature was in most cases very close to the final value resulting from equation (29). The calculations were performed on a high-speed digital computing machine, and the iteration process was continued until the percentage error in final temperature was less than 1 percent.

Simplified Calculation Procedure

In order to determine the initial wall-temperature distribution required for the iterative solution of equation (29), a simplified computation for wall temperature was made. It was assumed that (1) the inside wall radiation heat flux was negligible compared with the convection, (2) the axial conduction was insignificant, (3) all the heat radiated from the nozzle was radiated directly to space (no heat was radiated to the nozzle from outside sources or from one section of the nozzle to another), and (4) the wall was very thin and highly conductive, so that no significant temperature or surface area difference existed between the inside and outside wall. The heat balance can then be expressed as

$$-Q_{C,i} + Q_{r,o} = 0 \tag{31}$$

or

$$-h(T_{ad} - T_w) + \epsilon\sigma T_w^4 = 0 \tag{32}$$

This equation was solved for wall temperature by the Newton-Raphson method of successive iterations (ref. 6). The wall-temperature distribution obtained from equation (32) was utilized as the initial guess of temperature for equation (29).

Another simplified calculation was made to determine the wall thickness required to maintain a specified outside wall temperature. For nozzles characterized by a large temperature drop across the nozzle wall, equation (32) was modified as follows:

$$-h(T_{ad} - T_{w,i}) + \epsilon\sigma T_{w,o}^4 = 0 \tag{33}$$

For one-dimensional heat conduction through the nozzle wall in the radial direction, equation (30) was modified to

$$b = \frac{k_w(T_{w,i} - T_{w,o})}{h(T_{ad} - T_{w,i})} \tag{34}$$

With the specification of outside wall temperature and the assumption of inside wall temperature, the value of wall thickness b that satisfied both equations (33) and (34) was determined by an iterative procedure.

ANALYSIS RESULTS

The nozzle wall-temperature distribution and heat flux were determined over a range of chamber pressure. Hydrogen with a chamber temperature of 4680° R was the propellant. The effect of nozzle wall emissivity on the temperature distribution was also investigated. The results are presented in curve form in this section of the report.

Temperature Distribution

The variation of nozzle wall temperature with area ratio for chamber pressures ranging from 20 to 1500 pounds per square inch is shown in figure 4 for the nozzle illustrated in figure 3. The inside and outside wall emissivities were specified as 0.8. Both the simplified and refined temperature distributions are presented. For the refined solution the inside wall temperature is shown. In the divergent portion of the nozzle it is immediately apparent that the agreement between the approximate and refined solutions is excellent. The maximum difference in temperature

between the two solutions is slightly less than 5 percent, and over most of the nozzle length the difference is much less than 5 percent. The average temperature difference over the range of pressure and area ratio investigated is approximately 1 percent. In contrast, in the convergent section of the nozzle significant differences in temperature level between the two solutions existed, particularly at low values of chamber pressure. This temperature difference arises primarily because the radiant heat flux from the reactor to the nozzle wall has been neglected in the simplified solution. As indicated in reference 1, this radiant heat flux can be an appreciable percentage of the total heat flux in the convergent section of the nuclear nozzle, and therefore lower wall temperatures would be expected if the radiant heat transfer is omitted from the heat balance. It should be noted, however, that for the chemical rocket the difference in the two solutions in the convergent section would be of the same order of magnitude as the difference in the divergent portion of the nozzle, inasmuch as the radiant heat transfer in the convergent section of the chemical rocket would be much less than that in the nuclear rocket.

Studies of nuclear-rocket systems have indicated that for most missions relatively high reactor power levels and therefore high nozzle chamber pressures are required to satisfy the payload requirements. If a chamber pressure of 400 pounds per square inch is taken as typical of the pressure level associated with nuclear-rocket nozzle design, figure 4 indicates that a wall temperature approaching the propellant chamber temperature exists at the nozzle throat. Values of wall temperature range from a maximum of approximately 4400° R at the throat to 2300° R at an area ratio of approximately 60. As expected, the temperature levels increase somewhat with increasing chamber pressure and decrease with decreasing chamber pressure.

Heat Flux

The variation of net heat flux to the nozzle wall corresponding to the temperature distributions previously shown is presented in figure 5 where the heat flux is plotted against area ratio for a range of chamber pressure from 20 to 1500 pounds per square inch. The convective heat flux, shown as a dashed curve, is the heat-flux distribution associated with the simplified solution. The solid curve represents the combined (convective, radiative, and axial conduction) heat flux utilized for the refined solution. Although the heat flux as a result of axial conduction is not shown separately, it was normally several orders of magnitude less than the convective heat flux. The solid curve (fig. 5) therefore can be considered as the heat flux arising from convection and thermal radiation only. It is interesting to note that, in the divergent section of the nozzle, a 40-percent difference in heat flux between the simplified and refined solutions exists in some cases. Since the heat flux is proportional to the temperature to the fourth power, it might be expected that

small changes in temperature (fig. 4) would result in large changes in heat flux. It can also be noted that the radiant heat transfer in the divergent portion of the nozzle reduces the combined heat flux below that of the convective flux alone. The integrated difference in the two curves represents the amount of heat ultimately radiated from the wall to space through the nozzle exit.

In the convergent section, the combined flux is higher than the convective heat flux. For example, at low values of chamber pressure (20 lb/sq in.), the combined flux is approximately 13 times as large as the convective heat flux at the nozzle inlet. The difference in heat flux is decreased as chamber pressure is increased. As stated previously, the relatively low values of heat flux observed in the simplified solution are the result of neglecting the radiant heat transfer from the reactor to the nozzle wall.

Emissivity Variations

The effect of wall emissivity on the wall-temperature distribution was investigated for a fixed chamber pressure of 400 pounds per square inch absolute and a reactor face emissivity of 1.0. Two emissivity computations were performed. Initially, the inside wall emissivity was held constant at a value of unity and the temperature distributions were determined for outside wall emissivities ranging from 1.0 to 0.2. The computation of wall-temperature distribution for the wall emissivity equal to unity $(T_{w,i})_{\epsilon_o=1.0}$ was taken as a reference or base, and the temperature distributions for other values of emissivity were plotted as ratios $\frac{T_{w,i}}{(T_{w,i})_{\epsilon_o=1.0}}$ against outside wall emissivity for three nozzle positions corresponding to the inlet, the throat, and the exit in figure 6. As expected, the temperature ratio increased as emissivity decreased, because the amount of heat that can be radiated from the nozzle is proportional to the outside wall emissivity (eq. (32)). On a percentage basis, this effect (increased temperature with decreased emissivity) is greatest at the nozzle exit and smallest at the nozzle throat primarily because of the temperature levels associated with these nozzle positions. The nozzle throat is associated with a temperature of approximately 4000° R, and the nozzle exit temperature is of the order of 2000° R. Since the heat flux is a function of the fourth power of the temperature, a change in heat flux (effected by a change in emissivity) will result in a much smaller change in temperature at high temperatures than at low temperatures.

In the other computation, the outside wall emissivity was held constant, and the variation of temperature ratio with inside wall emissivity at the inlet, throat, and exit of the nozzle was determined (fig. 7). At

the nozzle throat essentially no variation in wall temperature was observed over the range of emissivity investigated. In contrast, a slight redistribution of radiant energy occurred at the inlet and exit of the nozzle in that the temperature ratio increased 4 percent and decreased 5 percent at the exit and inlet sections, respectively. The average temperature level of the nozzle, however, remained essentially unaffected by variations in the inside wall emissivity.

RADIATION-COOLED-NOZZLE FEASIBILITY AND REQUIREMENTS

Thus far, the analysis has been directed toward a nuclear-rocket nozzle with a thin highly conductive wall, and the results have indicated that these nozzles must operate at very high temperatures (approximately 4500° R). If conventional materials such as stainless steel or Inconel are to be utilized to withstand the structural loads, temperature levels of these materials must be maintained below 2000° R. Therefore, a thermal barrier, probably in the form of a nozzle liner, must be used in conjunction with the structural materials. One possible radiation-cooled-nozzle configuration is shown schematically in figure 8. The nozzle consists of a thin structural shell designed to withstand the pressure stress and a nozzle liner capable of withstanding high temperatures. These nozzles will be associated with wall thicknesses considerably larger than those considered in the previous analysis. Ideally, however, the nozzle liner should be characterized with a very low thermal conductivity (or correspondingly a large temperature drop per inch), so that the required liner thickness is kept to a minimum. Pyrolytic graphite and some of the metal oxides (e.g., zirconium oxide) satisfy both the temperature and the conductivity requirements and are therefore logical possibilities for such an application.

In order to determine the required liner thickness, the simplified solution for wall temperature was modified to account for the temperature drop across the liner, and the variation in the ratio of nozzle liner thickness to liner thermal conductivity with nozzle outside wall temperature was calculated at the nozzle throat from equations (33) and (34) for a chamber pressure of 400 pounds per square inch absolute. The results are shown in figure 9. These thicknesses represent the maximum values along the length of the nozzle. Thermal conductivities associated with logical nozzle liner materials range from 1×10^{-5} to 2×10^{-5} Btu/(sec)(in.)(°R). A conductivity of 1.5×10^{-5} Btu/(sec)(in.)(°R) was taken as representative of a typical liner, and the wall thickness corresponding to this conductivity is also shown in figure 9 for a range of outside wall temperature. The wall thickness is strongly dependent upon the outside wall temperature in that a change in wall temperature from 2000° to 3000° R reduces the wall thickness by approximately an order of magnitude (10 times).

At outside wall temperatures (2000° R) associated with nozzles designed with steel as a pressure shell, the required liner thickness at the throat would be approximately 1 inch. However, if one of the refractory metals (e.g., molybdenum, tantalum, or tungsten) is employed as the structural wall material, it may be possible to operate the nozzle wall at temperatures approaching 3000° R. Structural wall operating temperatures at this level reduce the nozzle liner thickness to a much more practical and desirable value of approximately 0.1 inch. It is felt that nozzles of this type will not weigh significantly more than regeneratively cooled nozzles.

In order to place the radiation-cooled nozzle in its proper perspective in relation to the nuclear-rocket powerplant, a comparison of the radiation-cooled nozzle and regeneratively cooled nozzle was felt to be desirable, since the regeneratively cooled nozzle is presently under development as a component of the nuclear rocket. A comparison of the impulse loss associated with the cooling of both nozzles was therefore evaluated. The integral of the heat-flux curves (convection plus radiation) of figure 5 over the nozzle area represents the energy transferred from the propellant to the nozzle wall and ultimately radiated to space. As in the case of the regeneratively cooled nozzle (ref. 1), this energy transfer represents a loss. However, the loss for the radiation-cooled nozzle is significantly less than that of the regeneratively cooled nozzle. This is illustrated in figure 10, where the specific-impulse gain associated with the radiation-cooled nozzle over the regeneratively cooled nozzle is plotted against nozzle chamber pressure. The regeneratively cooled nozzle described in reference 1 was used as a basis of comparison. It can be noted in the figure that the gain in specific impulse associated with the thin-walled radiation-cooled nozzle amounts to approximately 1 percent over the range of chamber pressure investigated. For radiation-cooled nozzles with nozzle liners that act as a thermal barrier, the impulse gain over the regeneratively cooled nozzle will be somewhat greater than the 1 percent indicated in figure 10, because the liner will reduce the heat transfer through the nozzle wall. If 10,000 pounds of propellant (which is considered a reasonable quantity) are required for a practical nuclear-rocket mission such as a lunar probe, the 1-percent gain in impulse shown in figure 10 would result in an increase in payload of approximately 100 pounds. An additional gain in impulse will result because of the elimination of the coolant pressure loss of the regeneratively cooled nozzle. If wall temperatures are limited to 2000° R for the regeneratively cooled nozzle, pressure drops across the nozzle cooling jacket can be expected to range from 200 to 300 pounds per square inch absolute. Since the turbopump requires approximately 1 percent of the propellant for every 800 pounds per square inch produced, elimination of the nozzle pressure drop will result in an impulse gain of 0.25 to 0.4 percent. The overall increase in impulse, then, as a result of decreased heat loss and system pressure drop that can be expected by utilizing a radiation-cooled nozzle rather than a regeneratively cooled nozzle is

approximately $1\frac{1}{2}$ percent. This percentage increase in impulse is considered quite significant. It is also probable that reduced pump pressure requirements will result in decreased turbopump weight.

It should be kept in mind that nuclear-rocket nozzle cooling at high chamber pressures will be accompanied by very large system pressure losses if a regenerative cooling system is used (ref. 1). In order to attain satisfactory cooling with reasonably low pressure drops, the regenerative cooling must be supplemented with either film cooling or a refractory nozzle coating. As discussed in reference 1, both film cooling and refractory coatings are associated with some serious development problems. For high chamber pressure applications, therefore, it may be easier to solve the radiation-cooled nozzle material problems than to develop reliable film cooling techniques or refractory coatings.

For the radiation-cooled nozzle, the problems of material selection are similar to the reactor material problems in that both components will operate at approximately the same pressures and temperatures. The nozzle, however, must accommodate much higher propellant velocities than the reactor. Considerable success has been achieved in the development of higher temperature high-pressure reactors. It is felt, therefore, that reliable radiation-cooled nozzles can also be developed.

SUMMARY OF RESULTS

An analysis was made to determine the feasibility of operating radiation-cooled nuclear-rocket nozzles with hydrogen as the propellant. Temperature distribution and heat fluxes along the nozzle were calculated by a simplified heat balance which included only the convection into the wall and the radiation from the wall and by a more refined technique in which the heat balance included, in addition to the convection to and radiation from the wall, the radiation inside the nozzle and the axial and radial heat conduction. The following analysis results were obtained:

1. The agreement between the simplified and refined solutions of temperature distribution was excellent in the divergent portion of the nozzle. The average temperature difference over the ranges of pressure and area ratio investigated was approximately 1 percent. In the convergent section large differences in temperature between the two solutions were observed because the radiant heat flux from the reactor to the nozzle was neglected in the simplified solution.

2. At chamber pressures associated with nuclear-rocket design (400 lb/sq in.), the wall temperature (4400° R) at the throat approached the rocket chamber temperature. At an area ratio of 60 the wall temperature was approximately 2300° R. The wall temperatures increased at higher

values of chamber pressure and, of course, decreased at lower values of chamber pressure. In view of the wall-temperature level, nozzle liners with low thermal conductivity that are capable of withstanding high gas temperatures are necessary to provide a thermal barrier for the nozzle wall structural material. Maximum liner thicknesses (at the throat) varied from 1 inch for steel pressure shells to 0.1 inch for refractory-metal pressure shells.

3. Increasing the outside wall emissivity decreased the wall temperature. In contrast, variations of the inside nozzle wall emissivity had little effect on the wall temperature.

4. Obviously, in the range of wall temperatures associated with radiation-cooled nuclear nozzles (2000° to 4000° R), both nozzle material selection and fabrication will be difficult. However, since radiation-cooled nozzles are simpler in concept and will probably result in performance gains in terms of specific impulse over regeneratively cooled nozzles, and because of the anticipated difficulty of regenerative cooling at high chamber pressure, a development effort appears to be desirable.

Lewis Research Center
National Aeronautics and Space Administration
Cleveland, Ohio, July 28, 1961

REFERENCES

1. Robbins, William H., Bachkin, Daniel, and Medeiros, Arthur A.: An Analysis of Nuclear-Rocket Nozzle Cooling. NASA TN D-482, 1960.

2. Hast, D. R.: The Ultra-Low Pressure Liquid Propellant Space Propulsion System. TN 58-218, WADC, June 1958.

3. Eckert, E. R. G., and Drake, Robert M., Jr.: Heat and Mass Transfer. Second ed., McGraw-Hill Book Co., Inc., 1959.

4. King, Charles R.: Compilation of Thermodynamic Properties, Transport Properties, and Theoretical Rocket Performance of Gaseous Hydrogen. NASA TN D-275, 1960.

5. Robbins, William H.: An Analysis of Thermal Radiation Heat Transfer in a Nuclear-Rocket Nozzle. NASA TN D-586, 1961.

6. Pipes, Louis A.: Applied Mathematics for Engineers and Physicists. Ch. V, McGraw-Hill Book Co., Inc., 1946.

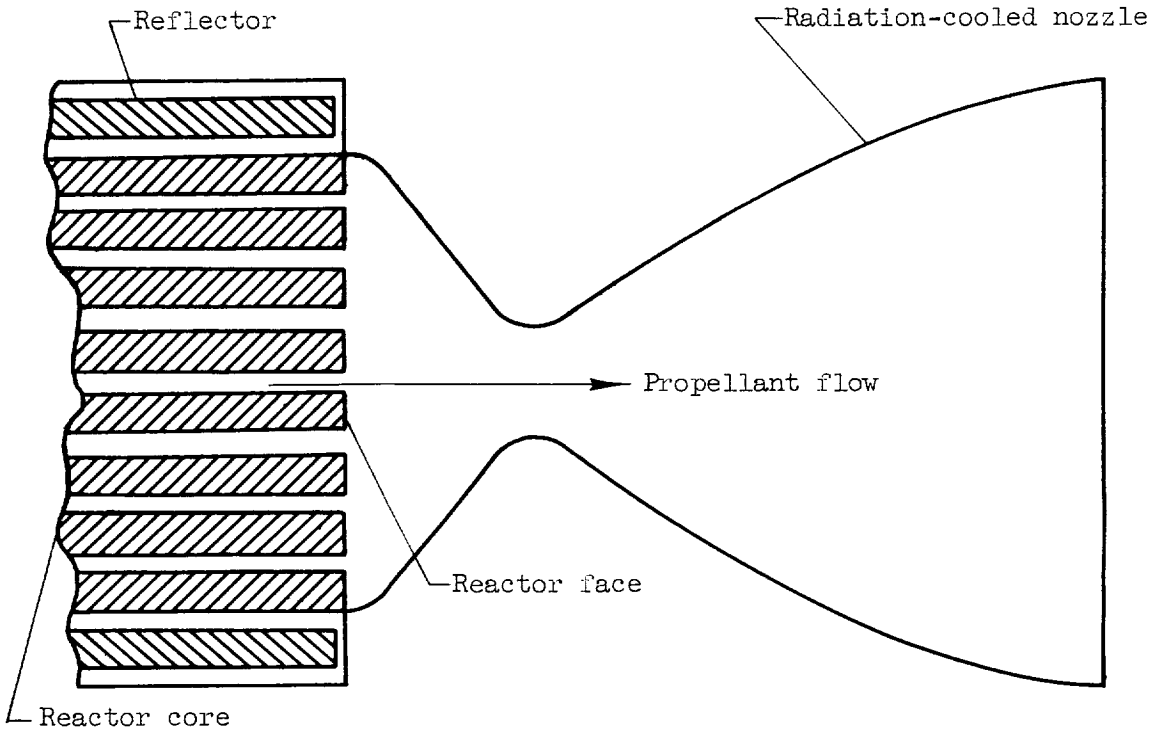

Figure 1. - Schematic diagram of nuclear rocket.

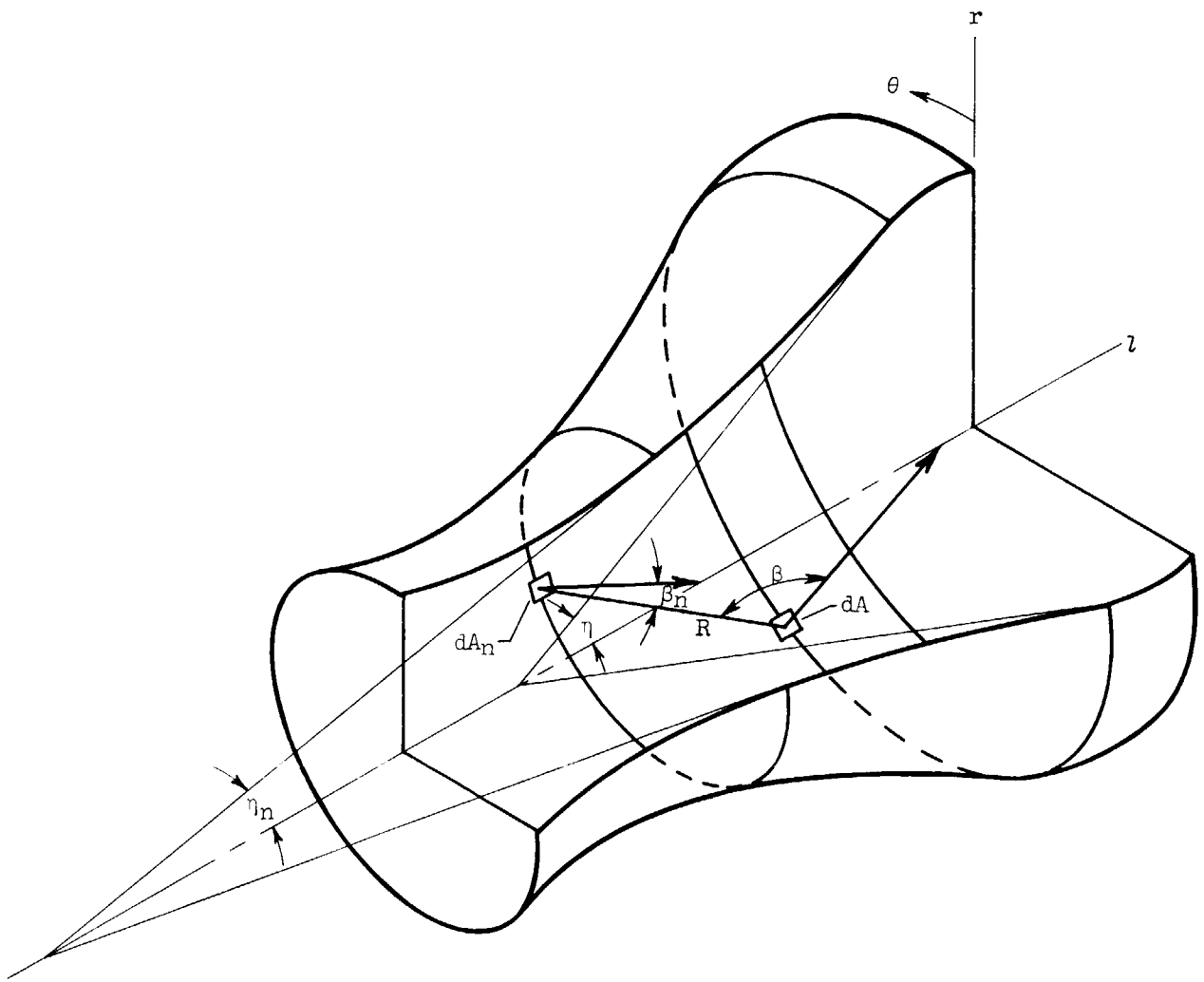

Figure 2. - Coordinate system for a general surface of revolution.

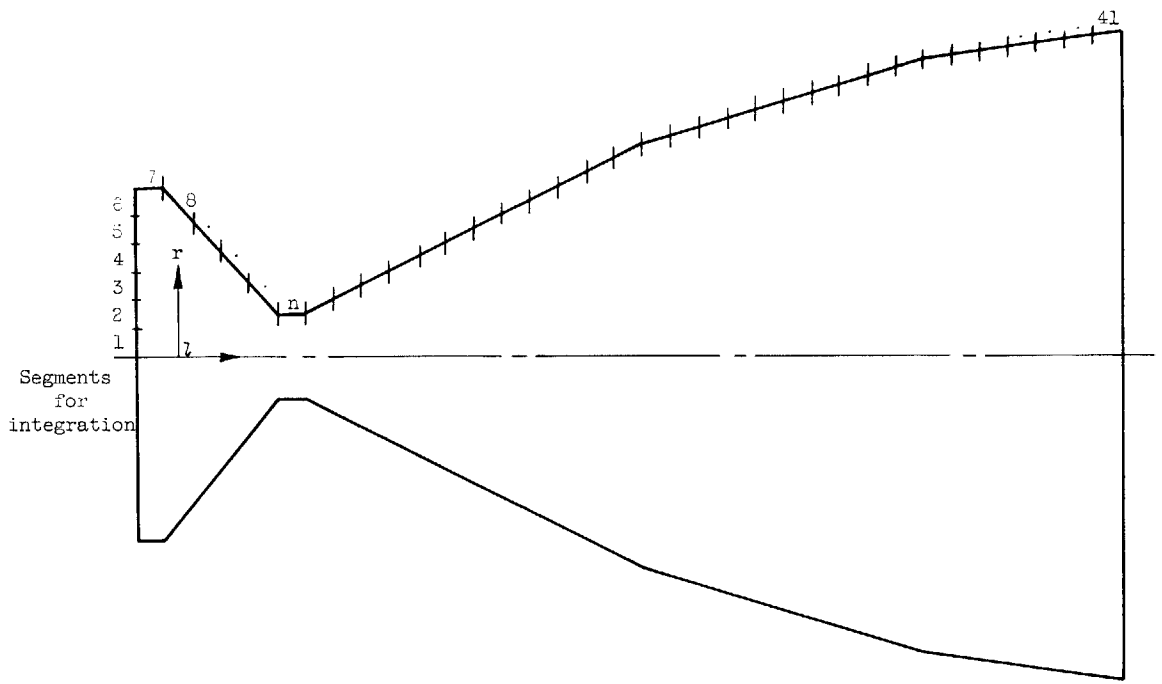

Nozzle coordinates

l, in.	r, in.
1	12.0
3	10.9
5	8.6
7	6.4
9	4.1
11	3.0
13	3.5
15	4.5
17	5.5
19	6.5
21	7.5
23	8.5
25	9.5
27	10.5
29	11.5
31	12.5
33	13.5
35	14.5
37	15.3
39	15.9
41	16.5
43	17.1
45	17.7
47	18.3
49	18.9
51	19.5
53	20.1
55	20.7
57	21.1
59	21.4
61	21.7
63	22.0
65	22.3
67	22.6
69	23.0

Figure 3. - Nozzle geometry. Wall thickness and material, 0.020-inch stainless steel; chamber temperature, 4680° R; throat diameter, 6 inches; ratio of inlet area to throat area, 16; ratio of exit area to throat area, 59; nozzle axial length, 70 inches.

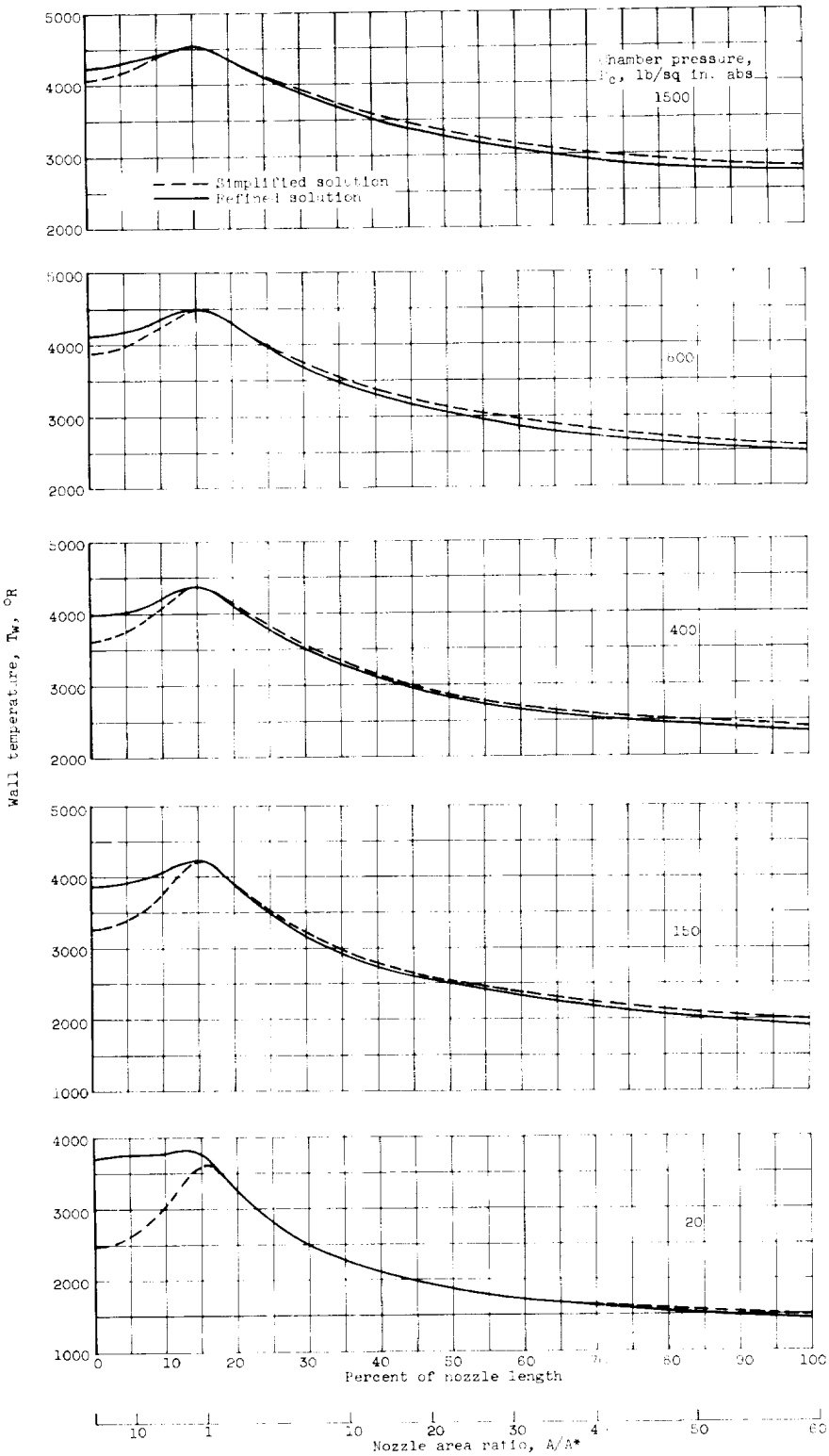

Figure 4. - Variation of nozzle wall temperature with nozzle length for various chamber pressures. Chamber temperature, T_c, 4000° R; inside and outside wall emissivities, $\epsilon_{w,i}$ and $\epsilon_{w,o}$, 0.8.

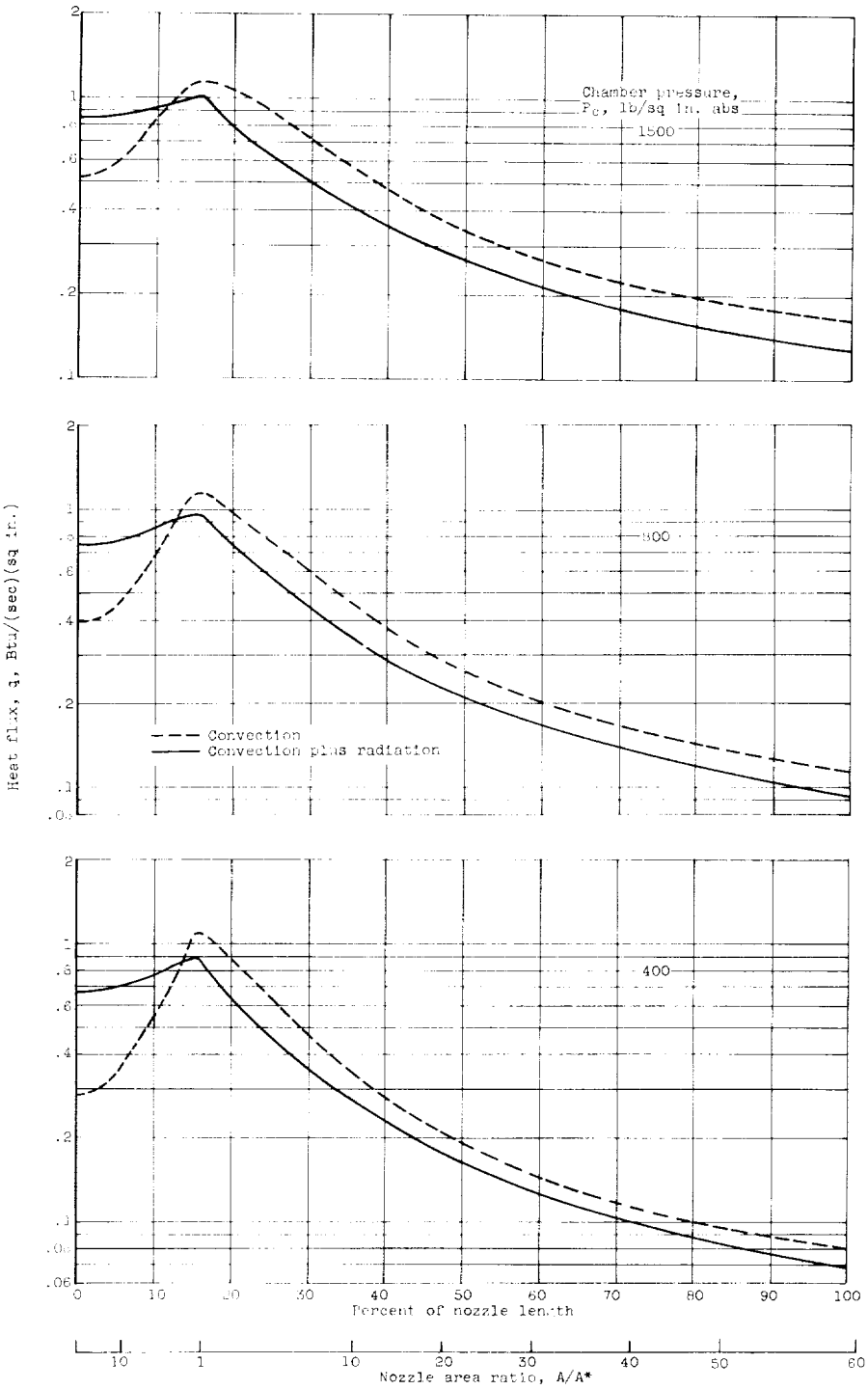

(a) Chamber pressure, 1500 to 400 pounds per square inch absolute.

Figure 5. - Variation of heat flux with nozzle length for various chamber pressures. Chamber temperature, T_c, 4680° R; inside and outside emissivities, $\epsilon_{w,i}$ and $\epsilon_{w,o}$, 0.4.

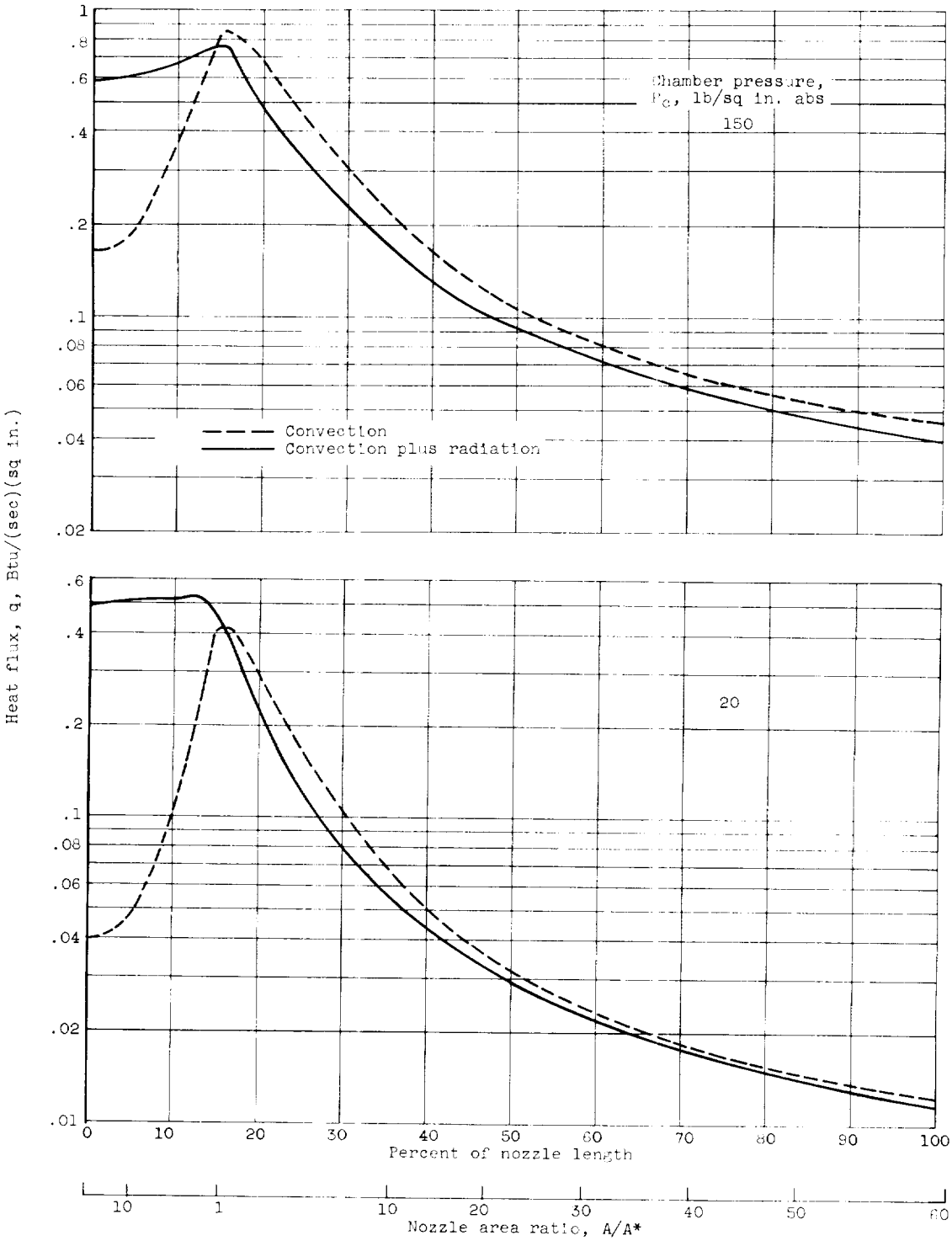

(b) Chamber pressure, 150 and 20 pounds per square inch absolute.

Figure 5. - Concluded. Variation of heat flux with nozzle length for various chamber pressures. Chamber temperature, T_c, 4680° R; inside and outside wall emissivities, $\epsilon_{w,i}$ and $\epsilon_{w,o}$, 0.8.

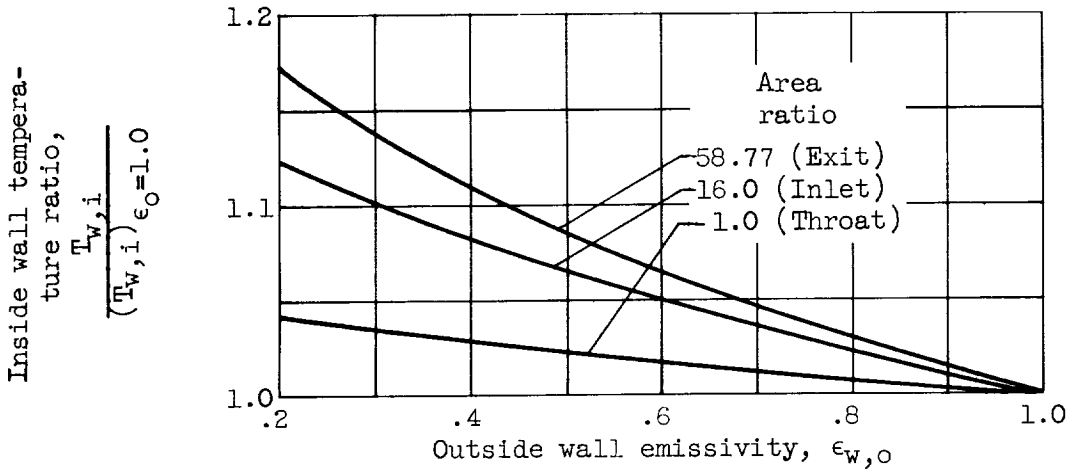

Figure 6. - Variation of inside wall temperature ratio with outside wall emissivity. Chamber pressure, P_c, 400 pounds per square inch absolute; inside wall emissivity, $\epsilon_{w,i}$, 1.0.

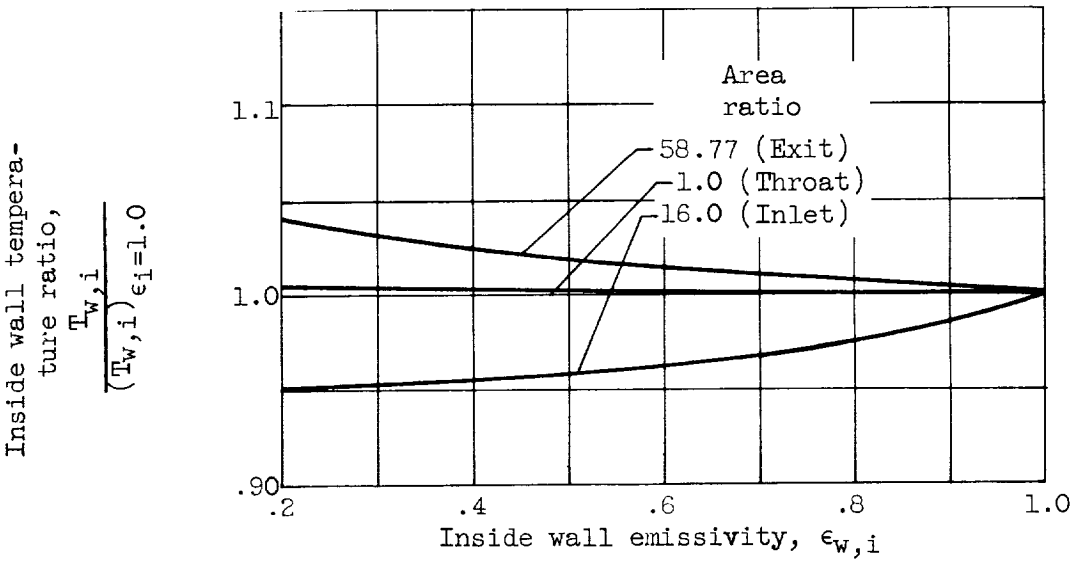

Figure 7. - Variation of inside wall temperature ratio with inside wall emissivity. Chamber pressure, P_c, 400 pounds per square inch absolute; outside wall emissivity, $\epsilon_{w,o}$, 1.0.

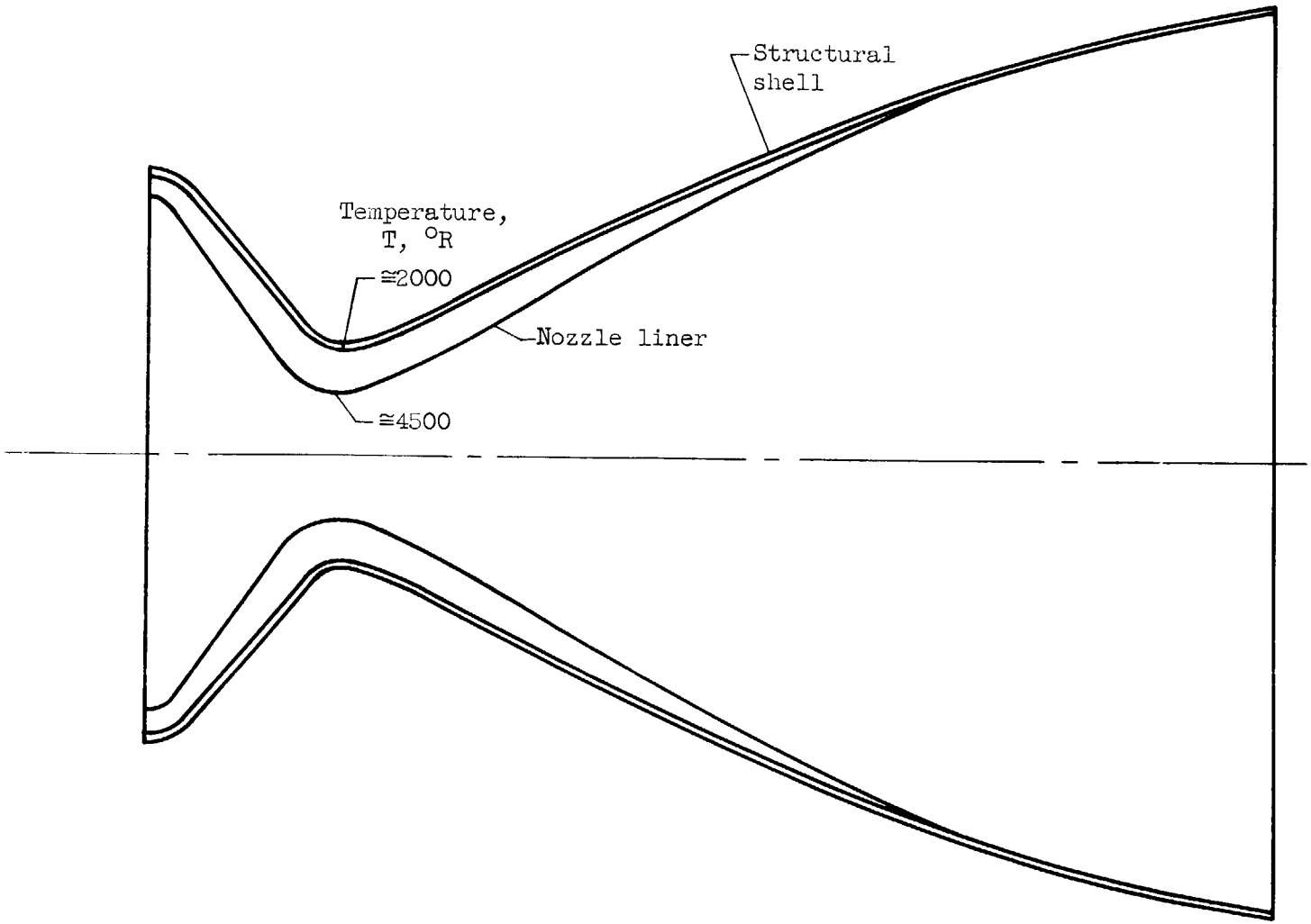

Figure 8. - Schematic diagram of radiation-cooled nuclear-rocket nozzle.

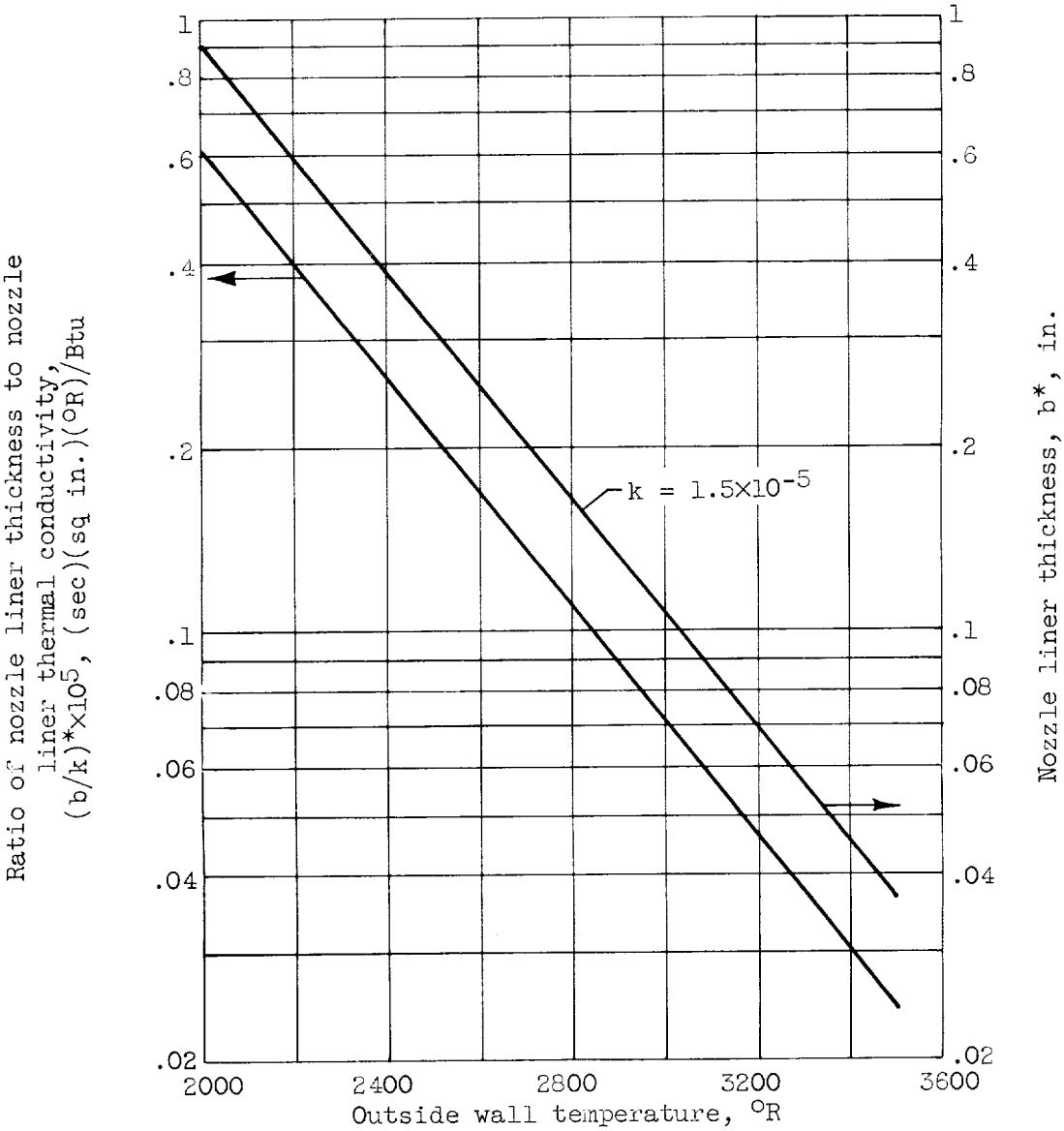

Figure 9. - Nozzle liner characteristics at nozzle throat for various outside wall temperatures. Chamber pressure, P_c, 400 pounds per square inch absolute; outside wall emissivity, $\epsilon_{w,o}$, 0.8.

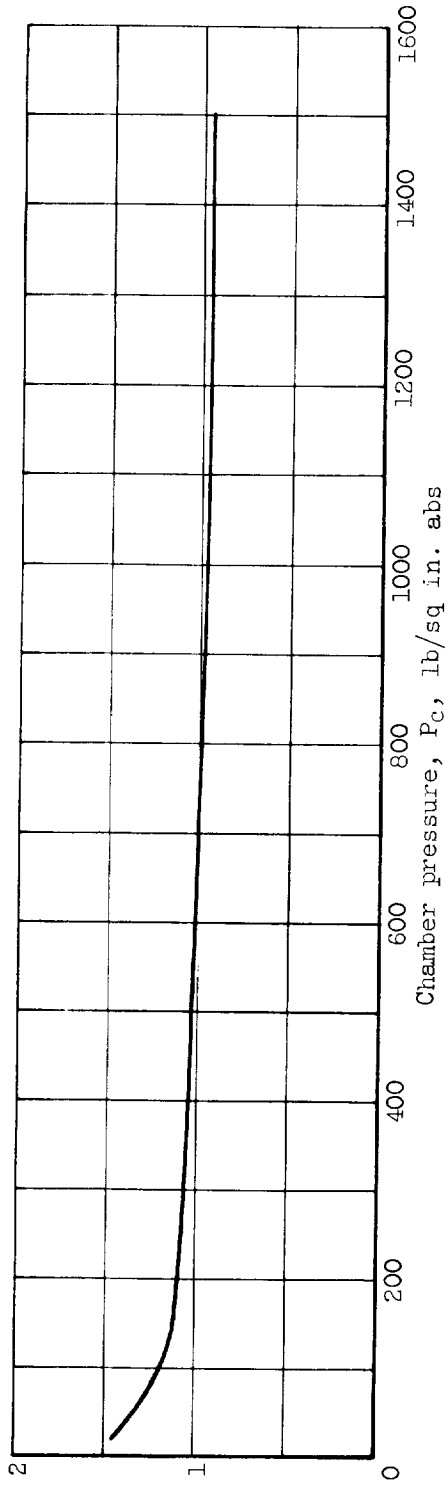

Figure 10. - Potential increase in specific impulse over regeneratively cooled nozzle associated with radiation-cooled nuclear-rocket nozzle.